Dual Enzyme-like Activities of Iron Oxide Nanoparticles and Their Implication for Diminishing Cytotoxicity

Zhongwen Chen,[†] Jun-Jie Yin,[‡] Yu-Ting Zhou,[‡] Yu Zhang,[†,*] Lina Song,[†] Mengjie Song,[†] Sunling Hu,[†] and Ning Gu[†,*]

[†]State Key Laboratory of Bioelectronics and Jiangsu Key Laboratory for Biomaterials and Devices, School of Biological Science & Medical Engineering, Southeast University, Nanjing, 210096, People's Republic of China, and [‡]Center for Food Safety and Applied Nutrition, Food and Drug Administration, College Park, Maryland 20740, United States

ABSTRACT

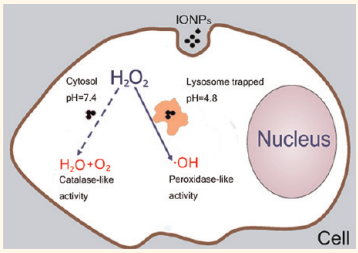

Iron oxide nanoparticles (IONPs) are frequently used in biomedical applications, yet their toxic potential is still a major concern. While most studies of biosafety focus on cellular responses after exposure to nanomaterials, little is reported to analyze reactions on the surface of nanoparticles as a source of cytotoxicity. Here we report that different intracellular microenvironment in which IONPs are located leads to contradictive outcomes in their abilities to produce free radicals. We first verified pH-dependent peroxidase-like and catalase-like activities of IONPs and investigated how they interact with hydrogen peroxide (H_2O_2) within cells. Results showed that IONPs had a concentration-dependent cytotoxicity on human glioma U251 cells, and they could enhance H_2O_2-induced cell damage dramatically. By conducting electron spin resonance spectroscopy experiments, we showed that both Fe_3O_4 and γ-Fe_2O_3 nanoparticles could catalyze H_2O_2 to produce hydroxyl radicals in acidic lysosome mimic conditions, with relative potency $Fe_3O_4 > \gamma$-Fe_2O_3, which was consistent with their peroxidase-like activities. However, no hydroxyl radicals were observed in neutral cytosol mimic conditions with both nanoparticles. Instead, they decomposed H_2O_2 into H_2O and O_2 directly in this condition through catalase-like activities. Transmission electron micrographs revealed that IONPs located in lysosomes in cells, the acidic environment of which may contribute to hydroxyl radical production. This is the first study regarding cytotoxicity based on their enzyme-like activities. Since H_2O_2 is continuously produced in cells, our data indicate that lysosome-escaped strategy for IONP delivery would be an efficient way to diminish long-term toxic potential.

KEYWORDS: iron oxide nanoparticles · cytotoxicity · ESR · hydroxyl radical · peroxidase · catalase

Iron oxide nanoparticles (IONPs) have been frequently used in a wide variety of biomedical applications, such as magnetic resonance imaging (MRI), drug or gene delivery, hyperthermia, and *in vivo* cell tracking.[1,2] In each case, cells of interest must be labeled with a relatively large amount of IONPs to be ready for diagnosis or treatment, thus raising the issue of toxicity concern.[3] In addition, nanocomposites containing iron were considered recently to be a new leverage against iron deficiency and may have a promising application in food science,[4−6] which even encourages a thorough evaluation of their biocompatibility. While many studies focus on cellular responses after exposure to nanoparticles (NPs), for example, inhibition of proliferation and differentiation, effect on cell morphology and functionality, or induced apoptosis and death,[7−12] little is reported that analyzes the chemical reactions on the surface of NPs as a source of cytotoxicity.

It is generally known that one important reason for IONP cytotoxicity is reactive oxygen species (ROS) generation and increased oxidative stress.[11,13−15] Under a normal cellular redox cycle, the ROS are continuously produced and effectively neutralized by natural antioxidants such as glutathione and specific enzymes.[16] However, an increased number of catalytic iron either on the surface of IONPs or released into cytoplasm will break the homeostasis by promoting free radical production through Fenton and/or Haber−Weiss reactions.[17−20] When functional coatings like dextran or chitosan are considered to reduce ion liberation and effective sequestration of free iron by various metal-binding proteins under physiological conditions,[21] the surface of IONPs may play a dominant role in ROS contribution because of their large surface volume ratio. Many research groups have observed increased oxidative stress induced by IONPs with various physicochemical properties by using fluorescent probes[22] or other biochemical methods.[23] However, the lack of specificity and the wide variety of cell lines made it impossible to compare different IONPs in terms of ROS generation ability. Thus the disparate results from several studies have made it difficult to make any general conclusions. γ-Fe_2O_3 and

* Address correspondence to zhangyu@seu.edu.cn, guning@seu.edu.cn.

Received for review January 20, 2012 and accepted April 24, 2012.

Published online 10.1021/nn300291r

Fe_3O_4 are two major magnetic nanomaterials. Due to the relatively higher saturation magnetization and simple step to synthesis, Fe_3O_4 was commercially available for mostly MRI and hyperthermia.[24] However, its ferrous ions may raise the toxic risk as well as be chemically unstable. Therefore, oxidized γ-Fe_2O_3 could be a superior candidate for long-term clinical applications.

One typical example of free radical production on the surface of IONPs is that they possess intrinsic peroxidase-like activity *in vitro*;[25] they can catalyze oxidation of a peroxidase substrate in an acidic solution in the presence of H_2O_2. Mechanism studies showed that IONPs first degrade H_2O_2 to produce hydroxyl radicals (•OH) which are then responsible for substrate oxidation.[26−28] Unlike natural HRP, IONPs almost lose peroxidase-like activity in a neutral pH; instead, in this study, we found that they directly catalyze H_2O_2 into water and oxygen in such a condition, named catalase-like activity.[29] Here raises a conflict whether peroxidase-like activity or catalase-like activity IONPs are present within cells. For the former, highly toxic •OH would be produced to raise oxidative stress, but for the latter, H_2O_2 would be decomposed into a biosafe species.

Therefore, we designed a protocol to investigate how IONPs may interact with H_2O_2 within cells. Human glioma U251 cells were first exposed to IONPs for efficient endocytosis and then treated with a low concentration of H_2O_2. We evaluated cell viability and examined hydroxyl radical production in different conditions to mimic a different intracellular microenvironment by using electron spin resonance spectroscopy (ESR) technology, the most powerful and direct analytical method for quantification of short-lived radicals. Since H_2O_2 is continuously produced in cells, our data may help to explain the cytotoxicity of IONPs on a nano-bio interfacial level and give implications to diminish it. Also the approaches developed in this paper may throw new light in evaluating ROS generation ability of other nanomaterials in the perspective of enzyme-like activities.

RESULTS AND DISCUSSION

Synthesis and Characterization of IONPs. γ-Fe_2O_3 NPs were synthesized according to a well-established coprecipitation procedure and then coated with dimercaptosuccinic acid (DMSA) molecules.[30] For Fe_3O_4, oleic acid (OA)-capped Fe_3O_4 was first synthesized by a modified coprecipitation method in a H_2O/DMSO mixing system, and DMSA was then used to replace OA to obtain water-soluble NPs.[31]

The physicochemical properties of both NPs investigated in this study are summarized in Table 1, including their ζ-potential and hydrodynamic diameters from a dynamic light scattering experiment at pH 4.8 acetic acid (HAc) buffer and pH 7.4 phosphate buffer solution (PBS). Both NPs have a similar core diameter (Figure 1) and hydrodynamic diameter. Due to the carboxyl groups on their DMSA coatings, both particles carry negative surface charges as reflected by a low negative ζ-potential. The surface area of particles is approximately 181.75 m^2/g iron for DMSA-Fe_2O_3 (D-Fe_2O_3) and 205.07 m^2/g iron for DMSA-Fe_3O_4 (D-Fe_3O_4) by calculation based on their core diameters. Since the surface area per quantitative iron of two IONPs was similar, we used the iron concentration to approximately represent the concentration of NPs in the following experimental protocols and discussions.

TABLE 1. Characterizations of IONPs

		ζ (mV)		hydrodynamic diameter (nm)	
particles	average core diameter (nm)	pH = 4.8	pH = 7.4	pH = 4.8	pH = 7.4
D-Fe_2O_3	9.0	−28.6 ± 2.3	−32.1 ± 3.5	64.3 ± 3.2	97.5 ± 5.6
D-Fe_3O_4	7.8	−24.7 ± 2.8	−29.2 ± 2.6	56.7 ± 2.7	78.9 ± 4.8

Uptake and Cytotoxicity of IONPs. The uptake of IONPs by U251 cells was verified using TEM. Both D-Fe_2O_3 and D-Fe_3O_4 NPs were largely taken up by cells after 12 h exposure. Figure 2 shows that the majority of IONPs are located in lysosomes, which is consistent with previous studies,[9,32−34] indicating an endocytotic mechanism for uptake. Additionally, the intracellular levels of IONPs were qualitatively proportionate to the concentrations of NPs incubated with cells through intracellular iron analysis[35] (data not shown).

The acute cytotoxicity effect of IONPs was then evaluated by a cell counting kit-8 (CCK-8) approach. U251 cells were incubated with various concentrations of D-Fe_2O_3 or D-Fe_3O_4 NPs for 24 h and then processed for CCK-8 incubation to determine cell viability. Results showed that D-Fe_2O_3 had little toxic effect on human glioma cells; the cells possessed a viability of more than 85% at all tested concentrations (Figure 3). In contrast, D-Fe_3O_4 NPs, showing to be more cytotoxic than D-Fe_2O_3, resulted in a concentration-dependent cytotoxicity of cells. The viability decreased by 9.8, 15.1, 28.5, and 33.6% ($p < 0.01$) at iron concentrations 12.5, 25, 50, and 100 μg/mL, respectively.

***In Vitro* Peroxidase-like and Catalase-like Activities of IONPs.** Accumulating evidence strongly suggests that many nanosized materials have the ability to induce the production of ROS, thus resulting in various biological effects.[9,11,15,18] At the lower basal level, ROS can be effectively neutralized by natural antioxidants; however, at a higher abnormal level, ROS will break the redox homeostasis and induce irreversible cell damage.[16] Cytotoxicity of IONPs also involves ROS generation and increased oxidative stress. It is generally known that iron can catalyze the degradation of H_2O_2 through

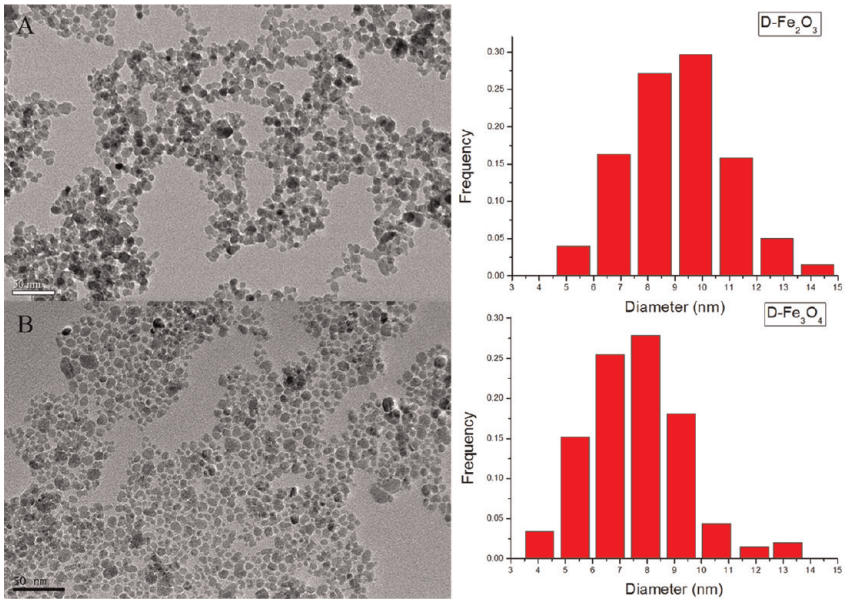

Figure 1. TEM images of (A) D-Fe_2O_3 and (B) D-Fe_3O_4 NPs.

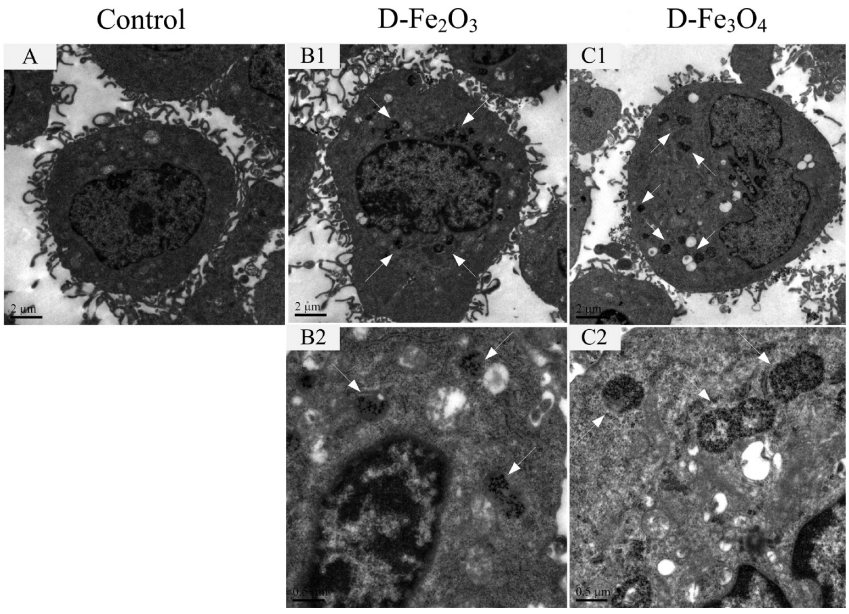

Figure 2. TEM images of U251 cells (A) without particles exposure and cells exposure to (B1,B2) D-Fe_2O_3 or (C1,C2) D-Fe_3O_4 NPs for 12 h, at an iron concentration of 100 μg/mL, with arrows indicating lysosomes containing the IONPs. The scale bar is 2 μm for top panel and 0.5 μm for bottom panel.

Fenton and/or Haber–Weiss reactions to produce hydroxyl radicals, which are highly toxic to cells, so the cytotoxicity of IONPs would significantly depend on the interactions between NPs and H_2O_2.

In recent years, Gao *et al.* found that magnetic nanoparticles possess an intrinsic peroxidase-like activity;[25] they are capable of catalyzing H_2O_2 to oxidize various peroxidase substrate. Mechanism studies demonstrated that IONPs first catalyze H_2O_2 to produce hydroxyl radicals, which are then responsible for substrate oxidation.[26−28] Therefore, one of the potential mechanisms involved in the cytotoxicity of IONPs could be their peroxidase-like activities. Once produced in cells, hydroxyl radicals would attack numerous intracellular molecules whichever could donate electrons, due to the lack of specificity.

In the present study, we investigated the peroxidase-like activities of D-Fe_2O_3 and D-Fe_3O_4 NPs in two intracellular pH conditions. At pH 4.8, both of them could catalyze the oxidation of substrate 3,3′,5,5′-tetramethylbenzidine (TMB) in the presence of H_2O_2, which was accompanied by color change to blue several minutes after IONPs were added into the H_2O_2/TMB reaction system (Figure 4A, tubes 2−5), as previously

reported.[25] Additionally, UV−vis absorption−time course curves indicated that D-Fe_3O_4 had a higher peroxidase-like activity than D-Fe_2O_3 under the same conditions (Figure 4B). However, the H_2O_2/TMB reaction solutions with both IONPs remained transparent instead of blue at pH 7.4 after 30 min incubation (Figure 4A, tubes 6 and 7), which suggested that IONPs did not exhibit peroxidase-like activity when pH reached neutral.

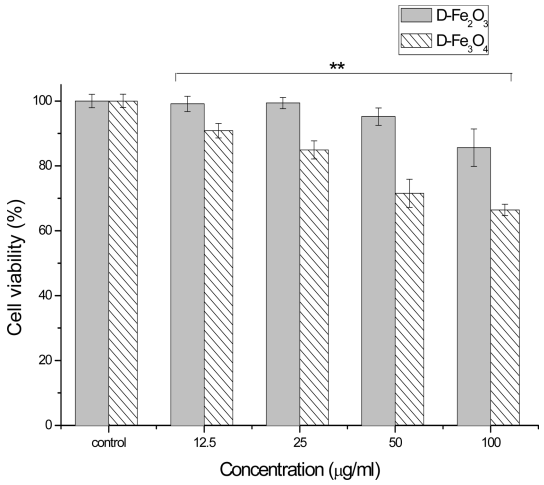

Figure 3. Cytotoxicity of IONPs. Cell viability was detected by the CCK-8 assay of human glioma U251 cells after 24 h treatment of D-Fe_2O_3 or D-Fe_3O_4 NPs. The data were normalized to control values (no particle exposure), which were set as 100% cell viability; $^{**}p < 0.01$, mean SEM, $n = 3$.

Instead, we found that IONPs possessed catalase-like activity in such a neutral condition. Gas bubbles were observed several minutes after H_2O_2 was added into tubes containing D-Fe_3O_4 NPs diluted with pH 7.4 PBS buffer and gradually grew bigger in the following hours (Figure 4C), indicating that D-Fe_3O_4 might behave similarly as catalase to decompose H_2O_2 into water and oxygen.[36] In contrast, bubbles were generated much slower as well as smaller for D-Fe_2O_3 NPs (Figure 4C, tube 2, with an arrow indicating very small gas bubbles). We further detected the catalase-like activity of D-Fe_2O_3/D-Fe_3O_4 NPs by monitoring dissolved oxygen in IONPs/H_2O_2 reaction systems (Figure 4D). The results demonstrated that both NPs could catalyze H_2O_2 to produce oxygen in PBS buffer, direct evidence of catalase-similar way to decompose H_2O_2. Consistent with their peroxidase-like activities, D-Fe_3O_4 also had a higher catalase-like activity than D-Fe_2O_3 NPs. A control experiment of dual enzyme activities of two NPs with the same size and high monodispersity synthesized through the thermal decomposition method was performed to verify the

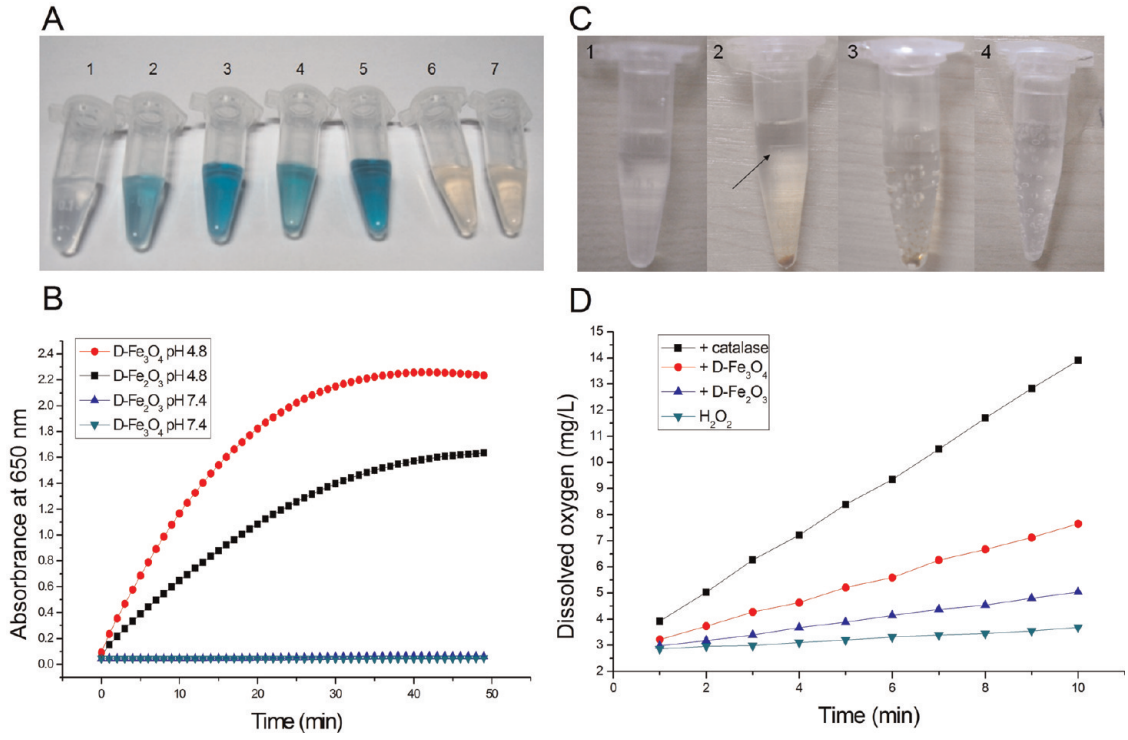

Figure 4. Peroxidase-like activity and catalase-like activity of IONPs. (A,B) Peroxidase-like activity of IONPs. (A) Photograph of color reactions after 30 min incubation. Tubes 1−5: H_2O_2 +TMB in pH 4.8 buffer plus (1) none, (2) 10 μg/mL D-Fe_2O_3, (3) 10 μg/mL D-Fe_3O_4, (4) 20 μg/mL D-Fe_2O_3, and (5) 20 μg/mL D-Fe_3O_4. Tubes 6 and 7: H_2O_2 + TMB in pH 7.4 buffer plus (6) 20 μg/mL D-Fe_2O_3 and (7) 20 μg/mL D-Fe_3O_4. (B) UV−vis absorption−time course curves of the TMB−H_2O_2 reaction system catalyzed by 20 μg/mL D-Fe_2O_3 or D-Fe_3O_4 NPs in pH 4.8 or 7.4 buffer. (C,D) Catalase-like activity of IONPs. (C) Photograph of bubble reactions after 6 h incubation. Tubes 1−4: 100 mM H_2O_2 in pH 7.4 PBS buffer plus (1) none, (2) 20 μg/mL D-Fe_2O_3 (arrow indicating very small bubbles), (3) 20 μg/mL D-Fe_3O_4, and (4) 20 U/mL catalase. (D) Dissolved oxygen−time course curves of H_2O_2 in pH 7.4 buffer catalyzed by 20 μg/mL D-Fe_2O_3 or D-Fe_3O_4 NPs or 20 U/mL catalase.

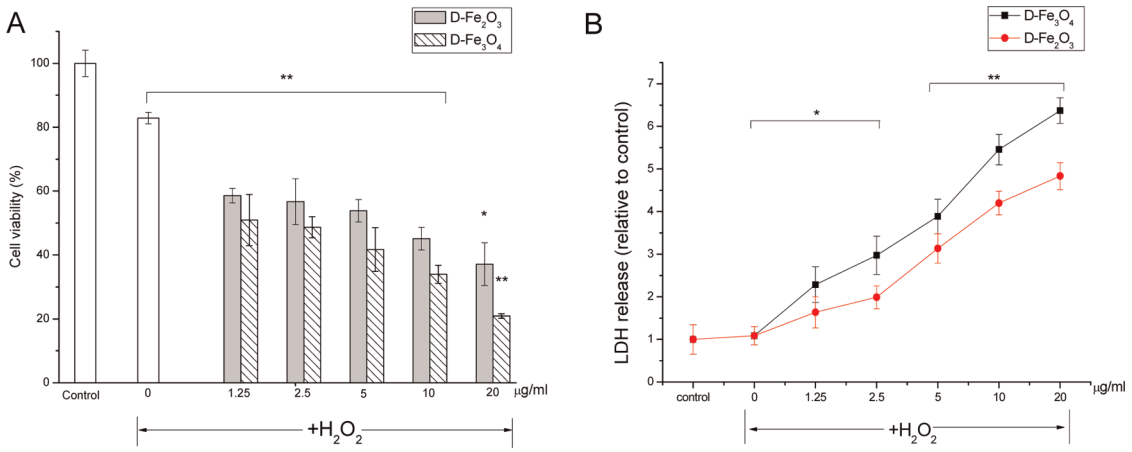

Figure 5. Effect of IONPs on cells in the presence of H_2O_2. The cells were incubated with 1.25−20 μg/mL IONPs for 12 h first and then treated with 30 μM H_2O_2 for another 4 h. Cell viability was detected by (A) CCK-8 assay and (B) LDH release assay. Data were normalized to controls; *$p < 0.05$, **$p < 0.01$, mean SEM, $n = 3$.

phenomena observed in Figure 4, which also has similar results (see Figure S1 in the Supporting Information).

According to our observations, whether peroxidase-like or catalase-like activity IONPs will be exhibited largely depends on their environmental pH, which is similar to previous studies on Pt-feritin nanoparticles[29] and Au@Pt nanostructures.[37] While in acidic conditions, IONPs could catalyze H_2O_2 to oxidize various substrates, they would rather decompose H_2O_2 directly into H_2O and O_2 in neutral conditions. Since peroxidase and catalase are two important categories of natural enzymes involved in regulating cellular redox homeostasis, we were then interested in which enzyme IONPs may act as in cells and its relationship with their cytotoxicity.

Effect of IONPs on Cells in the Presence of H_2O_2. H_2O_2 can be generated from several sources, for example, mitochondria, peroxisomes, and macrophages.[38] We intended to determine how IONPs may interact with H_2O_2 within cells, whether through peroxidase-like or catalase-like pathway. In physiological conditions, intrinsic peroxidase such as glutathione peroxidase can reduce H_2O_2 through oxidization of glutathione (GSH) to glutathione disulfide (GSSG), which can also be reduced back to GSH, forming a redox homeostasis cycle.[38] However, due to the lack of specificity, IONPs may catalyze H_2O_2 to react with various intracellular molecules including proteins, lipids, and nucleic acids through peroxidase-like activity, thus causing irreversible cell damage. In contrary, in the catalase-like pathway, IONPs would rather protect cells from oxidative stress through decomposition of H_2O_2 into H_2O and O_2.

In the present study, we designed a protocol to investigate the interactions between IONPs and H_2O_2 within cells. U251 cells were first exposed to IONPs for 12 h to obtain efficient endocytosis and then treated with 30 μM H_2O_2 for another 4 h. Cell viability was detected to evaluate their combined effects. The CCK-8 assay showed that both D-Fe_2O_3 and D-Fe_3O_4 NPs could enhance H_2O_2-induced cell damage dramatically (Figure 5A). Previous IONP exposure at an iron concentration of as low as 1.25 μg/mL could lead to a significant decrease of cell viability induced by H_2O_2, and it decreased more when IONP concentrations were higher. D-Fe_3O_4 was more toxic than D-Fe_2O_3 in the presence of H_2O_2, which is consistent with their cytotoxicity trend without additional H_2O_2 treatment, suggesting that there might be some causal relationships between IONPs' reaction with H_2O_2 and their cytotoxicity.

The results of lactate dehydrogenase (LDH) release assays also revealed a concentration-dependent cytotoxicity of IONPs in the presence of H_2O_2 (Figure 5B), with toxic potency D-Fe_3O_4 > D-Fe_2O_3. The rise of released LDH indicated the breakdown of the cell membrane.[11] It is noteworthy that H_2O_2 alone would not result in a significant rise of LDH, possibly because of its low concentration, so the toxic potential was also much likely because of the reaction products by IONPs and H_2O_2.

In order to investigate cell damage mechanisms, Hoechst 33342/PI stain was used to distinguish cells between live, apoptotic, and dead. While no visible damage was observed in cells only treated with H_2O_2 (Figure 6), H_2O_2-combined D-Fe_3O_4 NP treatments would directly lead cell to death (red) rather than apoptosis (no dark blue), indicating that increased amounts of D-Fe_3O_4 NPs would destroy cellular self-protecting networks against H_2O_2-induced oxidative stress in a very acute way.

On the basis of our previous hypothesis, these results implied that IONPs did not exhibit catalase-like activity in cells in that H_2O_2 was not decomposed to reduce cytotoxicity. Instead, IONPs might function in a peoxidase-like way to raise oxidative stress and damage cells. The possible explanation is that most IONPs were located in lysosomes, as observed by TEM (Figure 2), so that the acidic environment would contribute to their peroxidase-like activity rather than catalase-like activity as stated above.

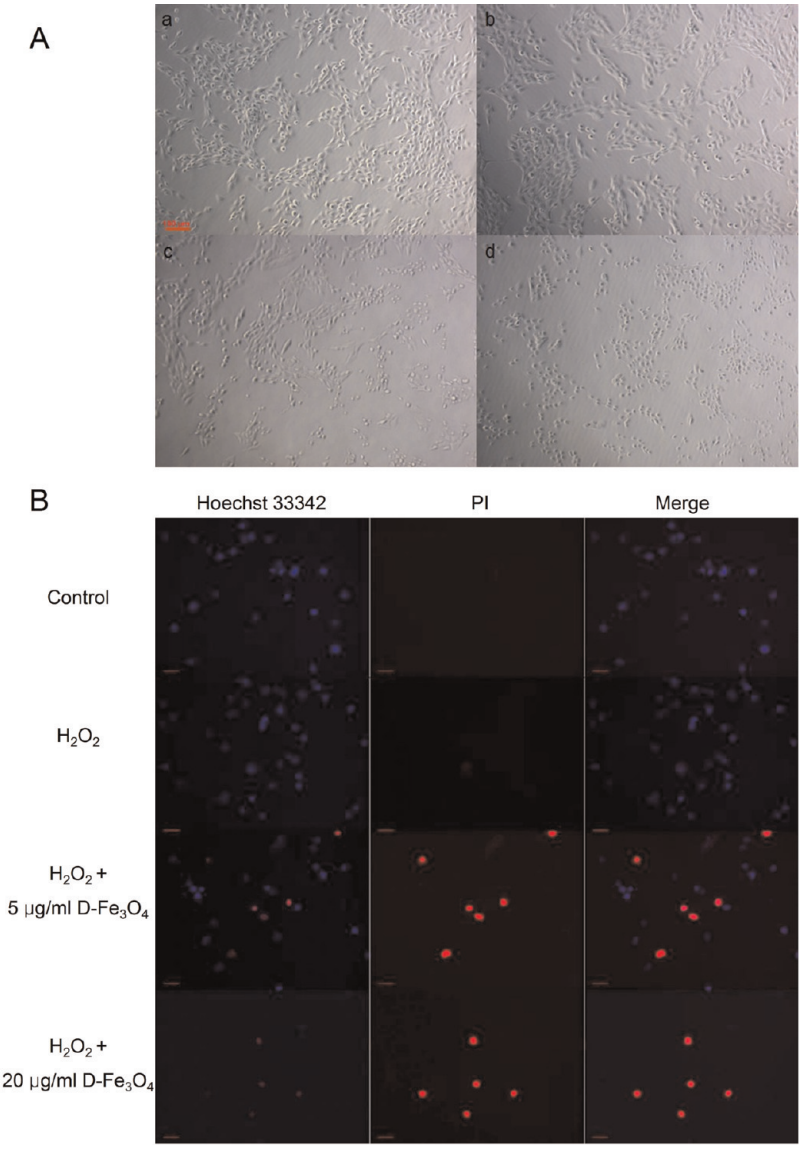

Figure 6. Images of cells treated by D-Fe_3O_4 NPs in the presence of H_2O_2. The U251 cells were incubated in D-Fe_3O_4 NPs for 12 h before 30 μM H_2O_2 treatment. (A) Optical microscope images of cells in the order of (a) control, (b) H_2O_2 treated only, (c) 5 μg/mL D-Fe_3O_4 nanoparticle exposure plus H_2O_2 treatment, and (d) 20 μg/mL D-Fe_3O_4 nanoparticle exposure plus H_2O_2 treatment. Scale bar: 100 μm. (B) Fluorescent microscopy image of live (in light blue) and dead (in red) cells stained through Hoechst 33342/PI. Scale bar: 20 μm.

According to hierarchical oxidative stress model,[15] under physiological concentrations, ROS act as signaling molecules mediating cell growth, migration, and differentiation. However, under a sustained environmental stress, ROS will accumulate to result in significant damage to cell structures and functions and may induce somatic mutations and neoplastic transformation.[39] Therefore, the long-term toxic risk of IONPs, especially for Fe_3O_4 NPs, should be carefully considered in biomedical applications, including MRI and cell labeling. Keenan *et al.* found that zero-valent iron nanoparticles could induce cell damage in the presence of oxygen through oxidation of iron, but the damage could be effectively limited by addition of ligands that prevented ferrous oxidation or when nanoparticles were oxidized prior to exposure to cells.[40] Our results also indicated that oxidized γ-Fe_2O_3 NPs was less toxic than Fe_3O_4 in the presence of H_2O_2 because of their lower peroxidase-like activity; therefore, γ-Fe_2O_3 could be safer for long-term clinical applications since H_2O_2 is continuously produced in cells.

Study of Free Radical Formation by ESR. ESR technique was employed to investigate the possible mechanism of cell damage by determining free radical production induced by IONPs in the presence of H_2O_2 in various conditions. At room temperature, the magnetic properties of the two IONPs were investigated by ESR (Figure 7) at pH 4.8 and 7.4 to mimic the environment of lysosome and cytosol, respectively. Noteworthy, both NPs exhibited different broad line shape of ESR spectra at pH

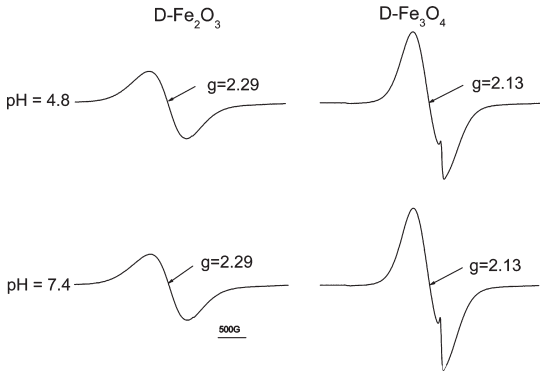

Figure 7. ESR spectra of D-Fe_2O_3 and D-Fe_3O_4 nanoparticle solutions. ESR measurements were carried out at room temperature under the following conditions: microwave power 20 mW, modulation amplitude 5 G, and scan range of 4000 G.

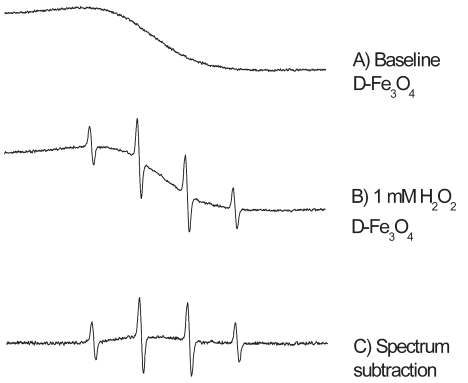

Figure 8. Demonstration of spectrum subtraction to obtain an ESR signal of spin adducts DMPO/•OH. Spectrum of solution containing (A) 50 mM DMPO and 20 μg/mL D-Fe_3O_4 in 100 mM acetate buffer (pH 4.8) and (B) 50 mM DMPO, 20 μg/mL D-Fe_3O_4, and 1 mM H_2O_2 in 100 mM acetate buffer (pH 4.8). Spectrum C was obtained through subtraction of spectrum A from B.

4.8 and 7.4. γ-Fe_2O_3 and Fe_3O_4 were known to possess superparamagnetic characteristics, and therefore, individual nanoparticles form strong interparticle dipolar interactions that provide effective spin relaxation mechanisms.[41,42] The *g* value of both D-Fe_2O_3 and D-Fe_3O_4 NPs remained the same at both acidic and neutral conditions, indicating that pH did not affect their superparamagnetic properties.

In this study of free radical formation by IONPs, we observed a weak ESR signal attributed to that of 5,5-dimethyl-1-pyrroline *N*-oxide DMPO/•OH superimposed on the portion of the signal from the superparamagnetic IONPs. This spectra overlapping were also mentioned in a previous study.[17] Figure 8B shows the complete 4 line spectrum (in 100 G range) of DMPO/•OH against a background derived from the partial spectrum of D-Fe_3O_4 NPs whose signal extends over 4000 G (Figure 7). In order to avoid the background due to the ESR spectrum from the IONPs themselves, centrifugation was used as described in previously reported work to separate IONPs from the reaction solution prior to ESR measurements.[17] In the present study, we intended to continuously monitor the progress of radical formation involving all possible sources surrounding the iron NPs during the entire time course of the experiment. Therefore, reaction solutions containing D-Fe_3O_4 NPs were directly measured during the collection of the ESR spectra. Then, ESR spectra of D-Fe_3O_4 NPs alone were obtained and used to subtract out the background due to D-Fe_3O_4 to clearly demonstrate the formation of DMPO/•OH (Figure 8C). In addition, the uneven baseline after subtraction (Figure 8C) rather than a straight line was possibly indicative of a physical or chemical change of D-Fe_3O_4 NPs during the reaction.

At pH 4.8, H_2O_2 alone did not produce hydroxyl radicals, as shown in Figure 9A. However, addition of IONPs assisted the formation of hydroxyl radicals from H_2O_2. The effect of NPs on the decomposition of H_2O_2 was further confirmed by the fact that the signal intensity of spin adducts DMPO/•OH was proportionally dependent on the concentration of both NPs. Compared with D-Fe_2O_3, much more radicals were yielded in the presence of D-Fe_3O_4, which suggested higher peroxidase-like activity of D-Fe_3O_4. In order to confirm their abilities to produce hydroxyl radicals that can react with organic molecules at pH 4.8, we observed the degradation of Rhodamine B, which can be oxidized by the hydroxyl radical to yield a photoinactive product (see Figure S2).[43]

The most likely reason for the formation of •OH was previously reported as Fenton-based reactions:[44]

$$Fe^{3+} + H_2O_2 \rightarrow FeOOH^{2+} + H^+ \quad (1)$$

$$FeOOH^{2+} \rightarrow Fe^{2+} + HO_2\bullet \quad (2)$$

$$Fe^{2+} + H_2O_2 \rightarrow Fe^{3+} + OH^- + OH\bullet \quad (3)$$

However, we surprisingly found that no signal of DMPO/•OH was observed at pH 7.4 in all samples (Figure 9B), which meant both NPs were not able to produce hydroxyl radicals at this pH, possibly because H_2O_2 was decomposed into H_2O and O_2 by IONPs through catalase-like activity. This was quite different from ferrous ions which are known to be able to catalyze H_2O_2 to produce hydroxyl radicals through formula 3 at a neutral pH, indicating new catalytic pathways of iron on the surface of NPs, which should be further investigated. At least, these results suggested that IONPs might not contribute to produce ROS at neutral pH.

Effect of IONPs on H_2O_2-Induced ROS at Cytosol Mimic Environment. IONPs were found to possess peroxidase-like activity in acidic pH, thus relating their ability of hydroxyl radical production to cytotoxicity when taken up into lysosomes discussed in previous sections. However, what effect might IONPs have on cells if they were not trapped in lysosomes? As is stated above that IONPs possessed catalase-like activity and did not

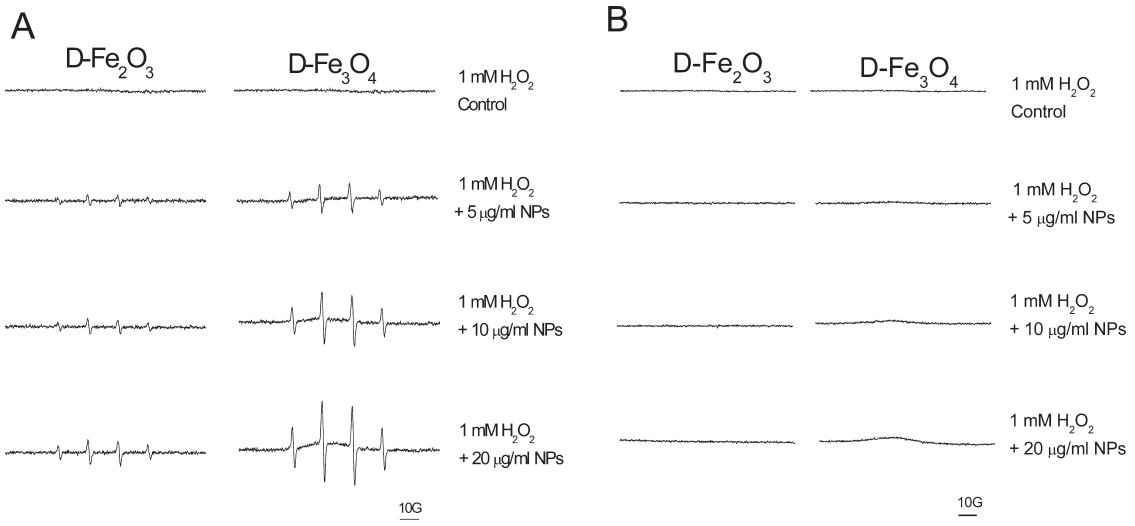

Figure 9. ESR spectra subtraction of spin adduct DMPO/•OH. All mixtures contained zero (control) or IONPs at different concentrations and 50 mM DMPO in (A) 100 mM acetate buffer (pH = 4.8) and (B) 50 mM PBS buffer (pH = 7.4). The reaction was initiated by adding 1 mM H_2O_2. ESR measurements were carried out at room temperature under the following conditions: microwave power 20 mW, modulation amplitude 1 G, and scan range of 100 G.

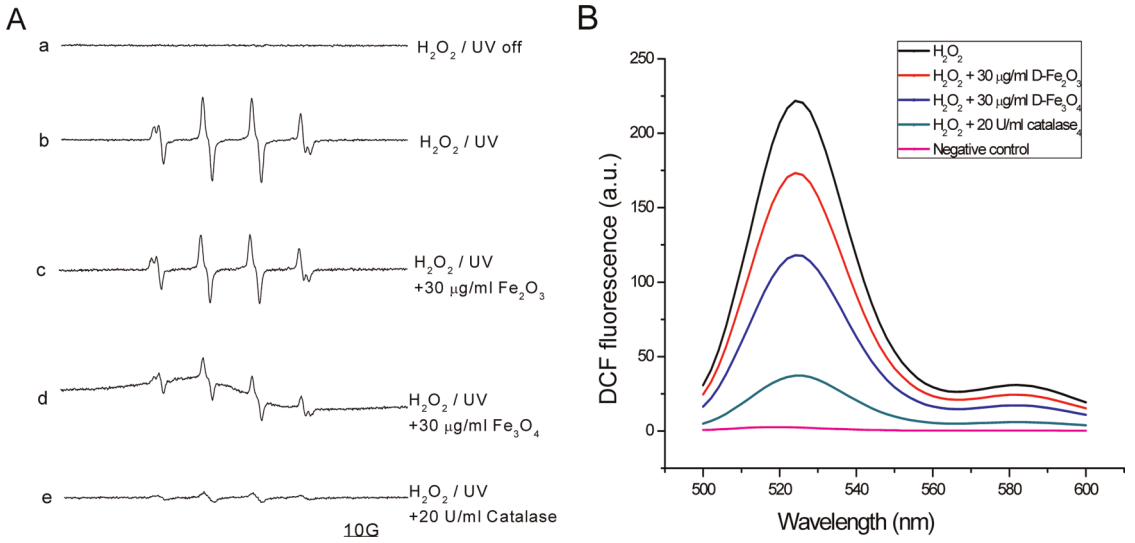

Figure 10. Effect of IONPs on H_2O_2-induced ROS at neutral environment. (A) Effect of IONPs and catalase on the formation of hydroxyl radicals in H_2O_2/UV system detected by ESR. All samples contained 25 mM BMPO and 5 mM H_2O_2 plus IONPs or catalase in 50 mM PBS buffer (pH 7.4). All mixtures except A were exposed to UV light for 15 min at 270 nm. The ESR intensity (peak to peak value) of the second line of each spectrum from b to e is 731, 595, 375, and 93 (in au), respectively. Spectra from sample c and d were obtained through spectrum subtraction. (B) Effect of IONPs and catalase on H_2O_2-induced ROS by detecting DCF fluorescence intensity. All samples contained 500 μM H_2O_2 and 10 μM H_2DCFDA plus IONPs or catalase in DMEM/FBS culture medium and were incubated at 37 °C for 30 min.

assist in producing hydroxyl radicals in neutral pH, we then evaluated their ability to protect cells in cytosol mimic conditions.

We first confirmed the decomposition of H_2O_2 by IONPs by monitoring its UV-irradiated hydroxyl radical products in pH 7.4 PBS buffer.[29] Because IONPs did not scavenge •OH in this condition (data not shown), the reduction of free radicals indicates the depletion of H_2O_2. After exposure to UV light, strong ESR signal of 5-*tert*-butoxycarbonyl 5-methyl-1-pyrroline *N*-oxide BMPO/•OH appeared (Figure 10Ab), while they diminished at different extents upon the addition of IONPs and catalase (Figure 10Ac–e). The reduction of signal intensity indicated that both types of IONPs could decompose H_2O_2 similarly as catalase, with higher effect of D-Fe_3O_4 than D-Fe_2O_3 at the same iron concentration.

It is well-known that, in neutral and alkaline pH, H_2O_2 itself tends to be decomposed into water and oxygen at a slow rate. The addition of iron oxides can actually accelerate this process.[45] The possible explanation is that, at higher pH, the reaction rate of formula 1 is higher, thus producing excessive $FeOOH^{2+}$ and

$HO_2\bullet$, the latter can then be ionized into O_2^- (formula 4). The formed $HO_2\bullet/O_2^-$ would immediately react with hydroxyl radicals to produce oxygen (formula 5).[46]

$$HO_2\bullet \rightarrow H^+ + O_2^- \quad (4)$$

$$OH\bullet + HO_2\bullet/O_2^- \rightarrow H_2O + O_2 \quad (5)$$

To explore the effect of IONPs on ROS production in neutral physiological conditions, we then used H_2DCFDA (2′,7′-dichlorofluorescein diacetate) fluorescence probe to detect ROS in IONPs/H_2O_2 reaction systems diluted with DMEM/FBS (fetal bovine serum) cell culture medium to mimic cytosol environment. Natural peroxidase contained in FBS can catalyze H_2O_2 to oxidize H_2DCFDA, thus forming a strong fluorescence (Figure 10B). However, the fluorescence intensity diminished by addition of IONPs or catalase, with higher effect of D-Fe_3O_4 than D-Fe_2O_3. Considering the negligible peroxidase-like activity of IONPs at this pH discussed above, these data indicated that IONPs could compete with natural peroxidase to decompose H_2O_2 through a catalase-like pathway in cytosol mimic solution to reduce H_2O_2-induced ROS production.

On the basis of the observations, we hypothesize that, if not trapped within acidic lysosomes when internalized into cells, IONPs may not contribute to raise cellular oxidative stress but protect cells through catalase-like activity in neutral cytosol. Therefore lysosome-escaped strategy for IONP delivery would be an efficient way to minimize long-term cytotoxicity of IONPs. In fact, there have been some approaches brought forward to deliver polymersomes or NPs into cells successfully escaped from lysosomes.[47,48]

CONCLUSIONS

In summary, we verified pH-dependent dual enzyme-like activities of IONPs. When internalized into cells, IONPs were mostly located in lysosomes and had a concentration-dependent cytotoxicity, with toxic potency D-Fe_3O_4 > D-Fe_2O_3. Both NPs can enhance H_2O_2-induced cell damage dramatically through peroxidase-like activity because of the acidic environment of lysosomes. γ-Fe_2O_3 NPs could be safer in biomedical applications since they produce a relatively lower amount of hydroxyl radicals compared with Fe_3O_4 in acidic conditions. However, both NPs do not produce hydroxyl radicals in neutral conditions but catalyze H_2O_2 into H_2O and O_2 directly through catalase-like activity. A scheme was shown to briefly describe the two ways IONPs may behave in cells (Figure 11). These results imply that the distribution and intracellular microenvironment of NPs are critical factors affecting their cytotoxicity and implicate that lysosome-escaped strategy for IONP delivery would be a promising method to diminish long-term toxic potential. The concept of enzymatic activity-based cytotoxicity could also be used for evaluating biotoxicity of other nanomaterials.

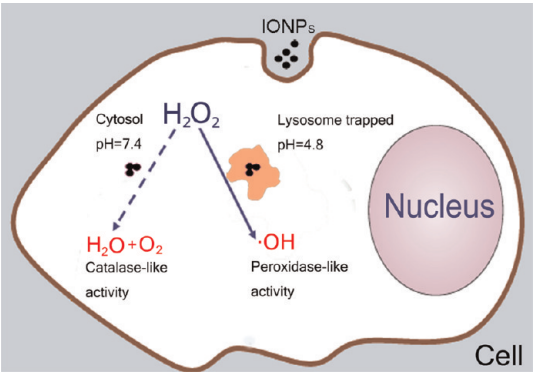

Figure 11. Schematic illustration of peroxidase-like activity-induced cytotoxicity by IONPs. IONPs are trapped in acidic lysosomes when internalized into cells, so they catalyze H_2O_2 to produce hydroxyl radicals through peroxidase-like activity; however, in neutral cytosol, IONPs would decompose H_2O_2 through catalase-like activity.

EXPERIMENTAL SECTIONS

IONP Synthesis and Characterization. γ-Fe_2O_3 and Fe_3O_4 NPs were synthesized and coated with DMSA molecules according to our previous work.[30,31] The core diameters of both NPs were then characterized by TEM (JEOL/JEM-2000E). Their ζ-potential and hydrodynamic diameters were detected by a zeta potential laser particle size analyzer (ZetaMaster3000, Marven).

Cytotoxicity of IONPs and H_2O_2 Treatment. Cytotoxicity of IONPs was analyzed by monitoring the mitochondrial reduction of CCK-8 kit (Dojindo Laboratories). Human glioma cells U251 (cultured in DMEM (Hyclone) supplemented with 10% fetal bovine serum (Gibco), 37 °C, 5% CO_2 atmosphere) were first plated at the amount of 1×10^4 cells/well in 96-well plates and settled overnight for adherence. Before exposure to cells, purified DMSA-Fe_2O_3 (D-Fe_2O_3) and DMSA-Fe_3O_4 (D-Fe_2O_3) nanoparticles were diluted in fresh medium at the concentration of 200 μg/mL, and then the diluted IONPs with fresh medium were added to wells to make a final concentration ranging from 12.5 to 100 μg/mL. After 24 h incubation, the medium was removed and the cells were rinsed once with fresh medium. Further procedures followed the instructions of the supplier.

To investigate the interactions of IONPs and H_2O_2 within cells, IONPs were first delivered into cells. Cells were plated at the amount of 1×10^4 cells/well in 96-well plates or 3×10^5 cells/well in 6-well plates and settled overnight for adherence. Different concentrations of D-Fe_2O_3 and D-Fe_3O_4 NPs were then added into wells for 12 h incubation. The medium was removed and rinsed once with medium, and 30 μM H_2O_2 diluted with DMEM without fetal bovine serum was then added. Cells were incubated for another 4 h at 37 °C, 5% CO_2 prior to being further analyzed.

Cell viability was assessed by the CCK-8 kit, and the supernatant medium in the wells was gathered for the released lactate dehydrogenase assay (LDH-kit, NJBI, China).

Live/Dead Cell Staining. Cells were plated as described above in 6-well plates. After IONP exposure and H_2O_2 treatment, cells were first washed with 10 mM phosphate buffer solution (PBS) once and then detached from the plate by trypsin. Hoechst

33342/PI was used from a live/apoptotic/dead cell detection kit (Keygentec, China) to stain cells. Each sample followed a staining of Hoechst 33342 at 37 °C for 15 min and PI at room temperature for 5 min and was then analyzed *via* fluorescent microscopy.

Transmission Electron Microscopy. Cells were plated as described above in 6-well plates. Twelve hours following exposure to IONPs at an iron concentration of 100 μg/mL, cells were detached and fixed overnight with 2.5% glutaraldehyde in 0.01 M PBS at 4 °C. The samples were then postfixed in 1% osmium tetroxide, dehydrated in ethanol, and embedded in Epon (Fluka). The ultrathin sections (60−80 nm) were stained with uranyl acetate and lead citrate and examined with a TEM (JEOL/JEM-2000E).

***In Vitro* Peroxidase-like Activity Assay.** The peroxidase-like activity assays were carried out in 1.5 mL tubes, with different concentrations (5, 10, 20 μg/mL) of D-Fe_2O_3/D-Fe_3O_4 in 0.5 mL of two reaction buffers (0.1 M pH 4.8 HAc buffer and 0.01 M pH 7.4 buffer), using 0.25 mg/mL 3,3′,5,5′-tetramethylbenzidine (TMB) as the substrate.[49,50] Blue color was observed several minutes after H_2O_2 was added, and photographs were taken at 30 min. The concentration of H_2O_2 used is 1.3 mM for photographs and 130 mM for UV−vis−NIR spectrophotometer monitoring on time-scan mode at 650 nm. All operations were done at room temperature and in the dark.

***In Vitro* Catalase-like Activity Assay.** The catalase-like activity assays were carried out in 1.5 mL tubes, with 20 μg/mL D-Fe_2O_3/D-Fe_3O_4 or 20 U/mL catalase diluted in 1 mL of pH 7.4 PBS buffer. Gas bubbles were observed several minutes after 100 mM H_2O_2 was added, and dissolved oxygen was monitored by a multi-parameter water quality meter (DZS-708, SHJK).

The catalase-like activity of IONPs was also evaluated in cell culture medium (DMEM + 10% FBS) to mimic cytosol environment. Twenty micrograms/milliliter D-Fe_2O_3/D-Fe_3O_4 and 10 μM H_2DCFDA fluorescence probe (2′,7′-dichlorofluorescein diacetate, Sigma) were added into 500 μM H_2O_2 diluted with culture medium. After 30 min incubation in 37 °C, the fluorescence of the medium was soon detected by a fluorescence spectrophotometer (Hitachi F-7000).

Electron Spin Resonance (ESR) Spectroscopy Measurements. ESR with a spin trapping technique was used to detect hydroxyl radicals (•OH) formed during the degradation of H_2O_2 induced by IONPs in various conditions. Because of its diamagnetic property, DMPO (5,5-dimethyl-1-pyrroline *N*-oxide, Dojindo) is capable of trapping these short-lived •OH and readily forming stable spin adducts DMPO/•OH. The characteristic ESR spectrum of the spin adduct was described in Zhao *et al.*'s study.[51] Each NP sample was mixed with DMPO in buffers of different pH values, and the reaction was triggered by addition of H_2O_2. The sample mixtures were transferred into a glass capillary and placed in the ESR cavity. The spectra for DMPO/•OH were collected at 8.5 min. Afterward, spectra subtraction between the sample mixtures with and without H_2O_2 solution was conducted to obtain a real ESR spectra signal of spin adducts DMPO/•OH.

In the H_2O_2/UV experiment, a light system consisting of a xenon lamp coupled with a Schoeffel monochromator (Chelmsford, MA) was used to generate UV light. It is well-known that hydrogen peroxide produces hydroxyl radicals under UV irradiation. Spin trap BMPO (5-*tert*-butoxycarbonyl 5-methyl-1-pyrroline *N*-oxide, Bioanalytical Lab) was used to trap the •OH to form the BMPO/•OH spin adduct, which yields the typical ESR spectrum with 1:2:2:1 intensity and hyperfine splitting of a_N = 13.47 G and a_H = 15.31 G. Samples were prepared at room temperature in PBS buffer (pH = 7.4) and transferred to a quartz capillary tube for ESR measurement. Each sample was UV-irradiated (270 nm power 500 W and distance 70 em) for 15 min, and spectra were recorded afterward.

All ESR measurements were carried out using Bruker EMX ESR spectrometer (Billerica, MA) at ambient temperature with 20 mW microwave power. Other settings are as follows: 1 G field modulation and 100 G scan range for detection of the DMPO and BMPO spin adducts, and 5 G field modulation and 4000 G scan range for detection of superparamagnetic IONPs (*g* value determination).

Statistical Analysis. Measurement for each treatment was repeated in triplicate, and the results were presented as mean SD (standard deviation). The statistical analysis of experimental data utilized the Student's *t* test. Each experimental value was compared to its corresponding control. Statistical significance was accepted when the probability of the result assuming the null hypothesis (*p*) is less than 0.05.

Conflict of Interest: The authors declare no competing financial interest.

Acknowledgment. This work was supported by the National Important Basic Research Program of China (No. 2011CB933503), the National Science Fund for Distinguished Young Scholars of China (60725101), the Basic Research Program of Jiangsu Province (No. BK2009013), the Special Funds of the National Natural Science Foundation of China for Basic Research Projects of Scientific Instruments (No. 61127002), and the China−U.S. International Science and Technology Cooperation Program (Grant No. 2009DFA31990). This article is not an official U.S. Food and Drug Administration (FDA) guidance or policy statement. No official support or endorsement by the U.S. FDA is intended or should be inferred. This work was supported by a regulatory science grant under the FY11 FDA Nanotechnology CORES Program (J.J.Y.)

Supporting Information Available: Peroxidase and catalase-like activities of monodisperse IONPs, and degradation of rhodamine B by peroxidase-like IONPs. This material is available free of charge *via* the Internet at http://pubs.acs.org.

REFERENCES AND NOTES

1. O'Grady, K. Progress in Applications of Magnetic Nanoparticles in Biomedicine. *J. Phys. D: Appl. Phys.* **2009**, *42*, 220301.
2. Berry, C. C. Progress in Functionalization of Magnetic Nanoparticles for Applications in Biomedicine. *J. Phys. D: Appl. Phys.* **2009**, *42*, 224003.
3. Soenen, S. J. H.; Himmelreich, U.; Nuytten, N.; De Cuyper, M. Cytotoxic Effects of Iron Oxide Nanoparticles and Implications for Safety in Cell Labelling. *Biomaterials* **2011**, *32*, 195–205.
4. Zimmermann, M. B.; Hilty, F. M. Nanocompounds of Iron and Zinc: Their Potential in Nutrition. *Nanoscale* **2011**, *3*, 2390–2398.
5. Miller, D. D. Food Nanotechnology: New Leverage against Iron Deficiency. *Nat. Nanotechnol.* **2010**, *5*, 318–319.
6. Hilty, F. M.; Arnold, M.; Hilbe, M.; Teleki, A.; Knijnenburg, J. T. N.; Ehrensperger, F.; Hurrell, R. F.; Pratsinis, S. E.; Langhans, W.; Zimmermann, M. B. Iron from Nanocompounds Containing Iron and Zinc Is Highly Bioavailable in Rats without Tissue Accumulation. *Nat. Nanotechnol.* **2010**, *5*, 374–380.
7. Soenen, S. J. H.; Nuytten, N.; De Meyer, S. F.; De Smedt, S. C.; De Cuyper, M. High Intracellular Iron Oxide Nanoparticle Concentrations Affect Cellular Cytoskeleton and Focal Adhesion Kinase-Mediated Signaling. *Small* **2010**, *6*, 832–842.
8. Soenen, S. J. H.; De Cuyper, M. Assessing Iron Oxide Nanoparticle Toxicity *in Vitro*: Current Status and Future Prospects. *Nanomedicine* **2010**, *5*, 1261–1275.
9. Lunov, O.; Syrovets, T.; Buchele, B.; Jiang, X. E.; Rocker, C.; Tron, K.; Nienhaus, G. U.; Walther, P.; Mailander, V.; Landfester, K.; *et al.* The Effect of Carboxydextran-Coated Superparamagnetic Iron Oxide Nanoparticles on c-Jun N-Terminal Kinase-Mediated Apoptosis in Human Macrophages. *Biomaterials* **2010**, *31*, 5063–5071.
10. Ankamwar, B.; Lai, T. C.; Huang, J. H.; Liu, R. S.; Hsiao, M.; Chen, C. H.; Hwu, Y. K. Biocompatibility of Fe_3O_4 Nanoparticles Evaluated by *In Vitro* Cytotoxicity Assays Using Normal, Glia and Breast Cancer Cells. *Nanotechnology* **2010**, *21*, 075102.
11. Apopa, P. L.; Qian, Y.; Shao, R.; Guo, N. L.; Schwegler-Berry, D.; Pacurari, M.; Porter, D.; Shi, X. L.; Vallyathan, V.; Castranova, V.; *et al.* Iron Oxide Nanoparticles Induce Human

Microvascular Endothelial Cell Permeability through Reactive Oxygen Species Production and Microtubule Remodeling. *Part. Fibre Toxicol.* **2009**, *6*, 1.
12. Pisanic, T. R.; Blackwell, J. D.; Shubayev, V. I.; Finones, R. R.; Jin, S. Nanotoxicity of Iron Oxide Nanoparticle Internalization in Growing Neurons. *Biomaterials* **2007**, *28*, 2572–2581.
13. Naqvi, S.; Samim, M.; Abdin, M. Z.; Ahmed, F. J.; Maitra, A. N.; Prashant, C. K.; Dinda, A. K. Concentration-Dependent Toxicity of Iron Oxide Nanoparticles Mediated by Increased Oxidative Stress. *Int. J. Nanomed.* **2010**, *5*, 983–989.
14. Soenen, S. J. H.; Illyes, E.; Vercauteren, D.; Braeckmans, K.; Majer, Z.; De Smedt, S. C.; De Cuyper, M. The Role of Nanoparticle Concentration-Dependent Induction of Cellular Stress in the Internalization of Non-toxic Cationic Magnetoliposomes. *Biomaterials* **2009**, *30*, 6803–6813.
15. Nel, A.; Xia, T.; Madler, L.; Li, N. Toxic Potential of Materials at the Nanolevel. *Science* **2006**, *311*, 622–627.
16. Ziech, D.; Franco, R.; Georgakilas, A. G.; Georgakila, S.; Malamou-Mitsi, V.; Schoneveld, O.; Pappa, A.; Panayiotidis, M. I. The Role of Reactive Oxygen Species and Oxidative Stress in Environmental Carcinogenesis and Biomarker Development. *Chem.-Biol. Interact.* **2010**, *188*, 334–339.
17. Smirnov, A. I.; Voinov, M. A.; Pagan, J. O. S.; Morrison, E.; Smirnova, T. I. Surface-Mediated Production of Hydroxyl Radicals as a Mechanism of Iron Oxide Nanoparticle Biotoxicity. *J. Am. Chem. Soc.* **2011**, *133*, 35–41.
18. Nel, A. E.; Madler, L.; Velegol, D.; Xia, T.; Hoek, E. M. V.; Somasundaran, P.; Klaessig, F.; Castranova, V.; Thompson, M. Understanding Biophysicochemical Interactions at the Nano-Bio Interface. *Nat. Mater.* **2009**, *8*, 543–557.
19. Valko, M.; Morris, H.; Cronin, M. T. D. Metals, Toxicity and Oxidative Stress. *Curr. Med. Chem* **2005**, *12*, 1161–1208.
20. Stohs, S. J.; Bagchi, D. Oxidative Mechanisms in the Toxicity of Metal-Ions. *Free Radical Biol. Med.* **1995**, *18*, 321–336.
21. Valko, M.; Rhodes, C. J.; Moncol, J.; Izakovic, M.; Mazur, M. Free Radicals, Metals and Antioxidants in Oxidative Stress-Induced Cancer. *Chem.-Biol. Interact.* **2006**, *160*, 1–40.
22. Barathmanikanth, S.; Kalishwaralal, K.; Sriram, M.; Pandian, S. R. K.; Youn, H.-S.; Eom, S.; Gurunathan, S. Anti-oxidant Effect of Gold Nanoparticles Restrains Hyperglycemic Conditions in Diabetic Mice. *J. Nanobiotechnol.* **2010**, *8*, 16.
23. Li, J. J.; Hartono, D.; Ong, C.-N.; Bay, B.-H.; Yung, L.-Y. L. Autophagy and Oxidative Stress Associated with Gold Nanoparticles. *Biomaterials* **2010**, *31*, 5996–6003.
24. Qiao, R.; Yang, C.; Gao, M. Superparamagnetic Iron Oxide Nanoparticles: From Preparations to *In Vivo* MRI Applications. *J. Mater. Chem.* **2009**, *19*, 6274–6293.
25. Gao, L. Z.; Zhuang, J.; Nie, L.; Zhang, J. B.; Zhang, Y.; Gu, N.; Wang, T. H.; Feng, J.; Yang, D. L.; Perrett, S.; *et al.* Intrinsic Peroxidase-like Activity of Ferromagnetic Nanoparticles. *Nat. Nanotechnol.* **2007**, *2*, 577–583.
26. Niu, H. Y.; Zhang, D.; Zhang, S. X.; Zhang, X. L.; Meng, Z. F.; Cai, Y. Q. Humic Acid Coated Fe_3O_4 Magnetic Nanoparticles as Highly Efficient Fenton-like Catalyst for Complete Mineralization of Sulfathiazole. *J. Hazard. Mater.* **2011**, *190*, 559–565.
27. Wang, N.; Zhu, L. H.; Wang, D. L.; Wang, M. Q.; Lin, Z. F.; Tang, H. Q. Sono-Assisted Preparation of Highly-Efficient Peroxidase-like Fe_3O_4 Magnetic Nanoparticles for Catalytic Removal of Organic Pollutants with H_2O_2. *Ultrason. Sonochem.* **2010**, *17*, 526–533.
28. Shin, S.; Yoon, H.; Jang, J. Polymer-Encapsulated Iron Oxide Nanoparticles as Highly Efficient Fenton Catalysts. *Catal. Commun.* **2008**, *10*, 178–182.
29. Fan, J.; Yin, J.-J.; Ning, B.; Wu, X.; Hu, Y.; Ferrari, M.; Anderson, G. J.; Wei, J.; Zhao, Y.; Nie, G. Direct Evidence for Catalase and Peroxidase Activities of Ferritin-Platinum Nanoparticles. *Biomaterials* **2011**, *32*, 1611–1618.
30. Liu, J. W.; Zhang, Y.; Chen, D.; Yang, T.; Chen, Z. P.; Pan, S. Y.; Gu, N. Facile Synthesis of High-Magnetization γ-Fe_2O_3/Alginate/Silica Microspheres for Isolation of Plasma DNA. *Colloids Surf., A* **2009**, *341*, 33–39.
31. Wu, Y.; Song, M.; Xin, Z.; Zhang, X.; Zhang, Y.; Wang, C.; Li, S.; Gu, N. Ultra-Small Particles of Iron Oxide as Peroxidase for Immunohistochemical Detection. *Nanotechnology* **2011**, *22*, 225703.
32. Noh, Y. W.; Jang, Y. S.; Ahn, K. J.; Lim, Y. T.; Chung, B. H. Simultaneous *In Vivo* Tracking of Dendritic Cells and Priming of an Antigen-Specific Immune Response. *Biomaterials* **2011**, *32*, 6254–6263.
33. Wilhelm, C.; Gazeau, F. Universal Cell Labelling with Anionic Magnetic Nanoparticles. *Biomaterials* **2008**, *29*, 3161–3174.
34. Kohler, N.; Sun, C.; Wang, J.; Zhang, M. Q. Methotrexate-Modified Superparamagnetic Nanoparticles and Their Intracellular Uptake into Human Cancer Cells. *Langmuir* **2005**, *21*, 8858–8864.
35. Ge, Y. Q.; Zhang, Y.; Xia, J. G.; Ma, M.; He, S. Y.; Nie, F.; Gu, N. Effect of Surface Charge and Agglomerate Degree of Magnetic Iron Oxide Nanoparticles on KB Cellular Uptake *in Vitro*. *Colloids Surf., B* **2009**, *73*, 294–301.
36. Day, B. J. Catalase and Glutathione Peroxidase Mimics. *Biochem. Pharmacol.* **2009**, *77*, 285–296.
37. He, W. W.; Liu, Y.; Yuan, J. S.; Yin, J. J.; Wu, X. C.; Hu, X. N.; Zhang, K.; Liu, J. B.; Chen, C. Y.; Ji, Y. L.; *et al.* Au@Pt Nanostructures as Oxidase and Peroxidase Mimetics for Use in Immunoassays. *Biomaterials* **2011**, *32*, 1139–1147.
38. Circu, M. L.; Aw, T. Y. Reactive Oxygen Species, Cellular Redox Systems, and Apoptosis. *Free Radical Biol. Med.* **2010**, *48*, 749–762.
39. Reuter, S.; Gupta, S. C.; Chaturvedi, M. M.; Aggarwal, B. B. Oxidative Stress, Inflammation, and Cancer: How Are They Linked. *Free Radical Biol. Med.* **2010**, *49*, 1603–1616.
40. Keenan, C. R.; Goth-Goldstein, R.; Lucas, D.; Sedlak, D. L. Oxidative Stress Induced by Zero-Valent Iron Nanoparticles and Fe(II) in Human Bronchial Epithelial Cells. *Environ. Sci. Technol.* **2009**, *43*, 4555–4560.
41. Bourlinos, A. B.; Simopoulos, A.; Petridis, D. Synthesis of Capped Ultrafine γ-Fe_2O_3 Particles from Iron(III) Hydroxide Caprylate: A Novel Starting Material for Readily Attainable Organosols. *Chem. Mater.* **2002**, *14*, 899–903.
42. Laurent, S.; Forge, D.; Port, M.; Roch, A.; Robic, C.; Vander Elst, L.; Muller, R. N. Magnetic Iron Oxide Nanoparticles: Synthesis, Stabilization, Vectorization, Physicochemical Characterizations, and Biological Applications. *Chem. Rev.* **2008**, *108*, 2064–2110.
43. Yu, F.; Xu, D.; Lei, R.; Li, N.; Li, K. a. Free-Radical Scavenging Capacity Using the Fenton Reaction with Rhodamine B as the Spectrophotometric Indicator. *J. Agric. Food Chem.* **2008**, *56*, 730–735.
44. Perez-Benito, J. F. Iron(III)-Hydrogen Peroxide Reaction: Kinetic Evidence of a Hydroxyl-Mediated Chain Mechanism. *J. Phys. Chem. A* **2004**, *108*, 4853–4858.
45. Gurol, M. D.; Lin, S. S. Hydrogen Peroxide/Iron Oxide-Induced Catalytic Oxidation of Organic Compounds. *J. Adv. Oxid. Technol.* **2002**, *5*, 147–154.
46. Kwan, W. P.; Voelker, B. M. Decomposition of Hydrogen Peroxide and Organic Compounds in the Presence of Dissolved Iron and Ferrihydrite. *Environ. Sci. Technol.* **2002**, *36*, 1467–1476.
47. Liu, G. J.; Ma, S. B.; Li, S. K.; Cheng, R.; Meng, F. H.; Liu, H. Y.; Zhong, Z. Y. The Highly Efficient Delivery of Exogenous Proteins into Cells Mediated by Biodegradable Chimaeric Polymersomes. *Biomaterials* **2010**, *31*, 7575–7585.
48. Boukany, P. E.; Morss, A.; Liao, W.-c.; Henslee, B.; Jung, H.; Zhang, X.; Yu, B.; Wang, X.; Wu, Y.; Li, L.; *et al.* Nanochannel Electroporation Delivers Precise Amounts of Biomolecules into Living Cells. *Nat. Nanotechnol.* **2011**, *6*, 747–754.
49. Zhang, X. Q.; Gong, S. W.; Zhang, Y.; Yang, T.; Wang, C. Y.; Gu, N. Prussian Blue Modified Iron Oxide Magnetic Nanoparticles and Their High Peroxidase-like Activity. *J. Mater. Chem.* **2010**, *20*, 5110–5116.
50. Huang, D.-M.; Hsiao, J.-K.; Chen, Y.-C.; Chien, L.-Y.; Yao, M.; Chen, Y.-K.; Ko, B.-S.; Hsu, S.-C.; Tai, L.-A.; Cheng, H.-Y.; *et al.* The Promotion of Human Mesenchymal Stem Cell

Proliferation by Superparamagnetic Iron Oxide Nanoparticles. *Biomaterials* **2009**, *30*, 3645–3651.
51. Zhao, H.; Joseph, J.; Zhang, H.; Karoui, H.; Kalyanaraman, B. Synthesis and Biochemical Applications of a Solid Cyclic Nitrone Spin Trap: A Relatively Superior Trap for Detecting Superoxide Anions and Glutathiyl Radicals. *Free Radical Biol. Med.* **2001**, *31*, 599–606.